Separation and physicochemical properties of residual carbon in gasification slag

Xiaoting Fan [1,2], Panpan Fan [1,2], Xiaodong Liu [1,2], Zhenyang Ren [1,2], Weiren Bao [1,2], Jiancheng Wang [1,2], Lianping Dong [3], Minqiang Fan [3]

[1] State Key Laboratory of Clean and Efficient Coal Utilization, Taiyuan University of Technology, Taiyuan 030024, China

[2] Key Laboratory of Coal Science and Technology(Taiyuan University of Technology), Ministry of Education, Taiyuan 030024, China

[3] College of Mining Engineering, Taiyuan University of Technology, Taiyuan 030024, China)

Corresponding author: fpp0313@126.com (Panpan Fan)

Abstract: Gasification slag is the solid waste produced in the coal gasification process, and its treatment and disposal problems are becoming more and more serious. In this study, the gasification slag produced in a chemical base in northern China and its residual carbon obtained by gravity separation of water medium were taken as the research objects, and their physicochemical properties were analyzed comprehensively. The residual carbon products, ash-rich products and high-ash products were obtained from the gasification slag after gravity separation. Under the optimal structure, the ignition loss of residual carbon products was reduced from 79.80% to 16.84%, and the yield was 11.64%. The high content of amorphous carbon and developed pores in the residual carbon provide the possibility of manufacturing high value-added materials. Raman spectrum showed that the residual carbon had lower aromaticity, higher content of small and medium aromatic ring structures, lower structural stability and easier combustion. Thermogravimetric combustion kinetics showed that the average combustion rate of residual carbon was $0.325(dm/dt)_{mean}/\% \cdot min^{-1}$, the comprehensive combustion characteristic index was $1.41 \cdot 10^{-9}\%^2 \cdot min^{-2} \cdot {}^{\circ}C^{-3}$. It has excellent performance and can be used as a raw material for mixed combustion in a circulating fluidized bed. The analysis of physical and chemical properties of residual carbon is of great significance for follow-up exploration of the resource utilization and high-value utilization of the residual carbon.

Keywords: waste treatment, gasification slag, physical and chemical properties, structural features, reaction kinetics

1. Introduction

Coal gasification technology is the foundation of the modern coal chemical industry and an effective way to achieve clean, efficient, green and low-carbon utilization of coal, and has important national strategic significance. Gasification slag is the solid waste generated in the coal gasification process, with an annual discharge of tens of millions of tons. According to incomplete statistics, the gasification slag emissions in the Ordos region alone exceeded 2 million tons in 2020 (Wang, 2021; Shi et al., 2020; Yu et al., 2020). At present, there is no mature method for large-scale consumption and resource utilization of gasification slag, most of which are landfill or accumulation treatment, which occupies a large amount of land. The leachate of heavy metals contained in the gasification slag will also cause soil and water pollution and seriously affected the local geological and ecological environment (Xu et al., 2009; He et al., 2014; Hu et al., 2016; Yang et al., 2013), which is an urgent problem for coal chemical enterprises.

The gasification slag includes the coarse slag discharged from the bottom of the gasifier and the fine slag carried by the gas flow from the top of the gasifier. The amount of gasification coarse slag accounts for about 80% of the total amount of gasification slag. Coal gasification slag contains a lot of inorganic minerals such as SiO_2, Al_2O_3, Fe_2O_3, CaO. The coal is not completely gasified in the gasifier resulting in the gasification slag containing some residual carbon. The residual carbon content in the gasification

coarse slag normally less than 10%, and the residual carbon content in the fine slag is relatively high, generally 30-40% (Zhu et al., 2019). The residual carbon can be mixed in boilers, but it is difficult to achieve high combustion efficiency and economic benefits due to its high moisture content (Chao et al., 2015). Coal gasification slag can be used as construction raw material to realize large-scale reuse of gasification slag (Pomykala, 2014), but due to the existence of carbon residue, the gasification fine slag is difficult to meet the loss on ignition (LOI)requirement as a building material, which restricts the LOI of building materials less than 8.0 % in the national standard code for Chinese characters GB/T 1596-2005, and it cannot even be used for road construction. Other uses, such as carbon/silicon-based adsorbents, catalyst (Florence et al., 2019), gel materials, compound material (Ayeni et al., 2022). These materials have a high added value, but a low market consumption. Abundant inorganic minerals and residual carbons provide the basis for their resource utilization, but their interdependent occurrence state limits their further utilization. Therefore, the separation of residual carbons and inorganic minerals in the gasification slag is a key prerequisite for realizing its large-scale and resource utilization.

The physical composition of fly ash is very similar to that of gasification slag (Blissett et al., 2012), so the separation technology of fly ash can be used for reference. Emre Altun et al. (Emre Altun et al., 2009) designed a new concurrent flow column for fly ash benefit, which can save about 80% of energy. Vassilev et al. (Vassilev et al., 2005) used dry magnetic separation to separate and recover magnetic concentrates from five kinds of fly ash produced by four large thermal power plants in Spain. The recovery rate of magnetic materials was 0.5%~18.1%. At present, the separation of residual carbon and inorganic mineral in gasification slag mainly includes flotation and gravity separation method. Hu et al. (Hu et al., 2018) and Liu et al. (Liu et al. ,2018) respectively used kerosene and 2＃oil as flotation agents to float residual carbon with a LOI of 88.92% and a carbon content of 85.03%, with yields of 16.12% and 21.81% respectively. The residual carbon were used to prepare activated carbon and treat methyl orange dyeing wastewater, the obtained products have good adsorption properties. Guo et al. (Guo et al., 2020) used the three-stage flotation method to separate the residual carbon with a yield of 52.65% and a LOI of 64.47%, and studied the micro pore difference and reaction activity between the gasification raw slag and the flotation residual carbon. It is considered that the developed pore structure of the residual carbon in the gasification slag enhances the adsorption of water and reagent of the gasification slag, which is the direct reason for the large consumption of flotation reagent (Xue et al., 2022; Liu et al., 2021).

At the same time, it is pointed out that a large number of oxygen-containing functional groups on the surface of gasification slag will reduce the hydrophobicity of the surface and improve the difficulty to adhesion to bubbles, and also lead to large dosage of reagent and poor flotation effect, which is temporarily not suitable for industrial application (Wu et al., 2020; Wang et al., 2021; Xue et al., 2021). The physical separation method-gravity separation can significantly improve the economy. In terms of the density difference between residual carbon and inorganic minerals in gasification slag, the researcher in Taiyuan University of technology first adopted the self-developed water-only cyclone to separate the gasification slag (Dong et al., 2018), which enabled effective separation of coarse particles, and applied for the patent of carbon and ash separation device and method (Dong et al., 2020). Li et al. (Li et al., 2021), Ren et al. (Ren et al., 2021) separated the coal gasification slag by using a complicated cone water medium cyclone with a compound cone structure to obtain residual carbon with LOI of 87.31%. The residual carbon was used to prepare carbon based activated coke with a mixing ratio of 50%. The desulfurization and denitration columnar activated coke meeting the excellent product index of national standard GB/T 30201-2013. The gravity separation is an economical and environmentally friendly method, with large processing capacity, simple equipment structure and higher comprehensive separation efficiency than flotation, and it is more advantageous for the separation and quality improvement of gasification slag.

The residual carbon in coal gasification slag has developed pore structure and larger specific surface area and average pore diameter. It is a special carbon source with low cost and easy access, and has the potential to prepare high value-added materials. However, due to the high difficulty of separation of carbon and ash from gasification slag, and the residual carbon obtained by the interfacial separation method is easily affected by residual auxiliary agents, there is few comprehensive physical property characterization of the residual carbon in coal gasification slag so far. In order to realize the

comprehensive utilization of gasification slag, this paper analyzes and tests the physical and chemical properties of the residual carbon separated and extracted from the gasification slag, in order to obtain the basic property database, so as to lay a foundation for the high-value utilization of residual carbon and the resource utilization of gasification slag.

2.   Materials and methods

2.1. Separation experiment of residual carbon

In this study, the dry pulverized coal gasification fine slag of Shenning furnace from a chemical base in northern China is selected as the separation object. The material properties and separation methods of the gasification fine slag are as described in the previous study (Ren et al., 2021). The slurry with a concentration of 100g/L is arranged in the mixing tank, and the feeding pressure is adjusted by the frequency converter. After the working conditions are stable, take overflow and underflow products at the same time. The overflow of the water-only cyclone is sieved by 0.074 mm, the product on the sieve is called residual carbon, and the under one is concentrated and filtered to be an ash-rich product. The underflow of the cyclone is high-ash product. The optimal cyclone parameters obtained in the previous test were selected and the ash content, yield and distribution rate of residual carbons were used as the evaluation indicators of the separation effect. The distribution rate of residual carbon in each product is defined by ε, and the calculation formula of ε is shown in (1):

$$\varepsilon = \frac{\gamma_j \, (100\text{-}A_j)}{100\text{-}A_y}$$
(1)

in which, γ_j is the product yield, %；A_j is the ash content of the product, %；A_y is the total ash content, %；ε is the carbon distribution rate, %.

2.2. Experimental instruments and methods

2.2.1. XRD analysis

The crystal structure of gasification slag and residual carbon was determined by X-ray diffractometer (MiniFlex 600, RIGAKU, Japan). Test conditions: Cu Target Kα Ray (λ=0.154056 nm), the scanning speed was 3°/min, the scanning step was 0.02°, the scanning range was 5~60°, the tube voltage is 40 kV, and the tube current is 15 mA.

2.2.2. FT-IR Spectrum analysis

The functional group structure of the gasification slag and residual carbon was analyzed by Fourier transform infrared absorption spectrometer(invenio-r, Bruker, Germany). The sample with a mass ratio of 1:200 was mixed with KBr and pressed into tablets. The infrared scanning range was 400-4000 cm^{-1} and the resolution was 4 cm^{-1}.

2.2.3. Pore Structure (low pressure gas adsorption) and SEM-EDS analysis

The pore structures of gasification slags and residual carbons were determined by a multifunctional nitrogen adsorption instrument (ASAP 2460, MICROMERITICS, USA). Take N_2 as the adsorbent, weigh about 1g sample and test it at 77 K and 0.1 MPa to obtain N_2 isothermal adsorption desorption curve.The BET model was used to calculate the total specific surface area in the sample, the BJH model was used to calculate the pore volume of the sample, and the t-plot model was used to calculate the micropores volume. Scanning electron microscope energy spectrometer (SEM-EDS，Rigaku MiniFlex 600) was used to observe the surface morphological characteristics of gasification slag and residual carbon.

2.2.4. Raman analysis

Structural characterization of gasification slags and residual carbons was carried out by laser confocal micro Raman spectrometer (inVia Reflex, RENISHAW, UK). An argon ion laser was used as the excitation light source with a laser wavelength of 514.5 nm and a resolution of 2 μm. The laser output

power is 20 mW, the power irradiated on the sample surface is 1 mW, the scanning range is 1800 – 800 cm^{-1}, and the scanning is 3 times.

2.2.5. Thermogravimetric analysis and combustion kinetics

The combustion properties of gasified slag and residual carbon were measured by thermogravimetric analyzer (TG/DTA7200, HITACHI, Japan) and the kinetics was studied. Heat from 30 °C to 900 °C, the heating rate is 5 °C/min, and the total air flow is 100 mL/min. The combustion atmosphere is an air atmosphere.

3.   Results and discussion

3.1. Influence of structural parameters on the effect of residual carbon separation

Referring to the previous condition test, fix the size of the underflow port of the cyclone and adjust the insertion depth of the overflow pipe of the cyclone to obtain the separation products under different working conditions. The influence of the insertion depth of the overflow pipe on the separation effect of the cyclone is shown in Fig. 1.

It can be seen from the above separation results that with the increase of the insertion depth of the overflow pipe, the separation density of the cyclone increased, the zero speed envelope moved down and more products enter to overflow, the ash content increases from 16.84% at 60 mm to 23.95% at 100 mm, and the yield increases from 11.64% to 15.13%. The ash content of the ash-rich products changed less because of the lower separation accuracy for the finer -0.074 mm particle size material. The LOI of the high-ash products obtained by separation was less than 2%. In terms of the carbon distribution rate,
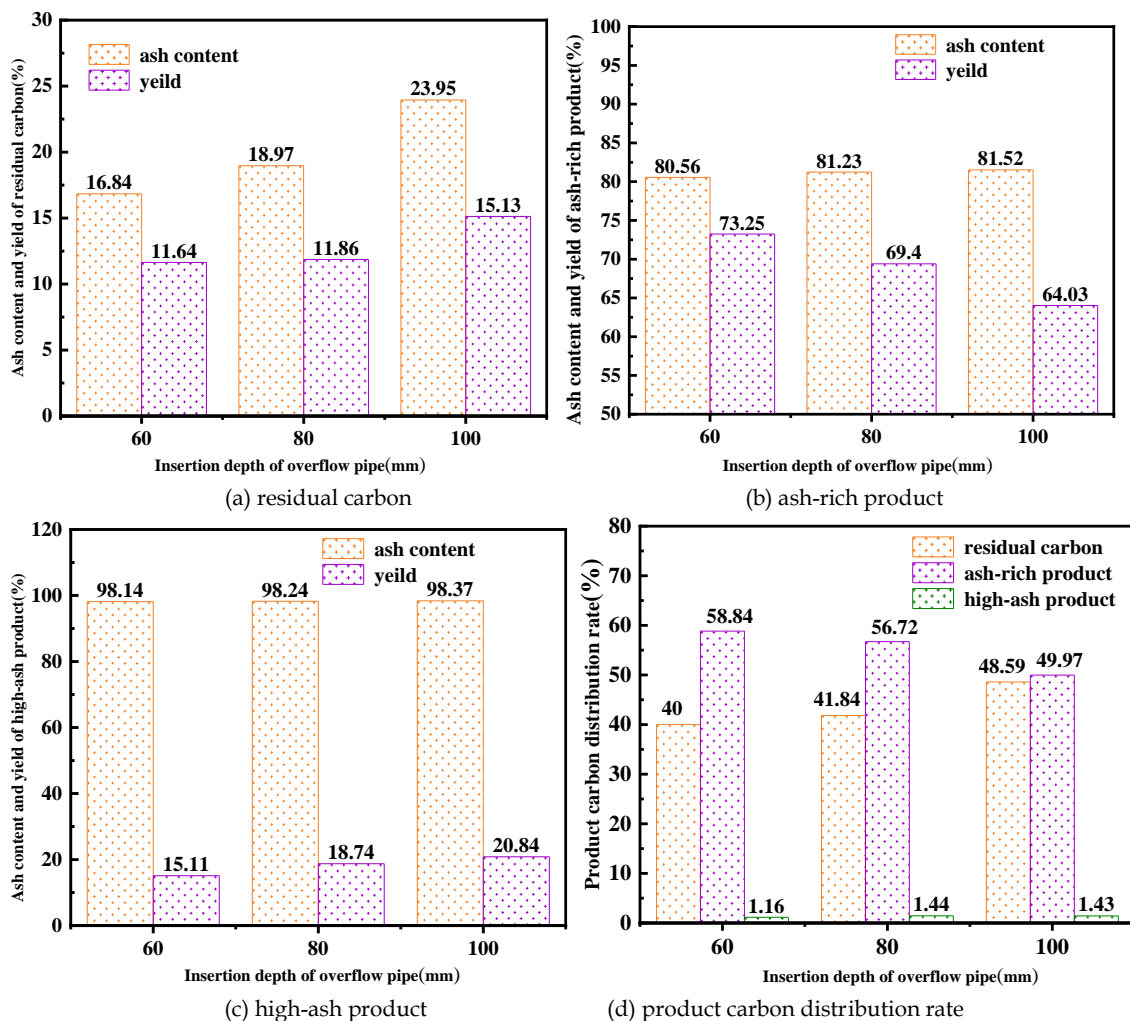

(a) residual carbon

(b) ash-rich product

(c) high-ash product

(d) product carbon distribution rate

Fig. 1. Separation effect of water medium cyclone with different insertion depth of overflow pipe

5

Physicochem. Probl. Miner. Process., 58(6), 2022, 154928

most of the carbon is enriched in the residual carbon products and ash rich products, and the residual carbon lost in the high-ash products accounts for less than 1.5%, indicating that the separation effect was good, and the test results were consistent with the test law obtained in the early stage.

It can be seen from the above separation effect that about 40.00%~48.59% of the carbon in the gasification slag can be efficiently enriched in the residual carbon product by gravity separation. In order to realize the high-value utilization of this product, this paper compares and analyzes the physical and chemical properties of the residual carbon products. Further fine separation of inorganic ash in ash-rich products will continue to be studied in follow-up work.

3.2. Analysis of physicochemical properties of residual carbon products

The research content of this part selects the residual carbon products under the test condition of 60 mm insertion depth of overflow pipe as the research object. The research scale carries out a series of physical and chemical property analysis from the perspective of macro appearance, mesoscopic characteristics, micro morphology and molecules, in order to obtain the full-scale basic physical properties of residual carbon components and lay a foundation for the high value-added utilization of residual carbon components.

3.2.1. Proximate and ultimate analysis

The proximate and ultimate analysis were performed on the gasification slag and residual carbon respectively, as listed in Table 1:

Table 1. Proximate and ultimate analysis of gasification slag and residual carbon

Sample	Proximate analysis /%				Ultimate analysis /%					Calorific value /(MJ·kg^{-1})
	M_{ad}	A_{ad}	V_{ad}	FC_{ad}	C	H	O*	N	S	Q_{grvd}
gasification slag	0.46	79.80	2.40	17.34	18.74	0.18	0.40	0.12	0.30	5.91
residual carbon	0.60	16.40	3.01	79.99	79.48	1.33	0.90	0.34	0.27	27.31

Note: *calculated by difference; M_{ad} is the moisture content on air dry basis; A_{ad} is the ash on air dry basis; V_{ad} is the volatile on air dry basis; FC_{ad} is the fixed carbon content, and Q_{grvd} is the calorific value.

The proximate analysis of gasification slag and residual carbon showed that the moisture of gasification slag on air drying basis was 0.46%, the ash content is 79.80%, and the volatile content of air drying basis was 2.40%, indicating that there was still a small amount of volatile content after high temperature gasification. The moisture of the air drying basis of the separated residual carbon is 0.60%, the ash content was reduced to 16.40%, and the fixed carbon content was increased to 79.99%, which provides a basis for subsequent high-value utilization.

3.2.2. Particle size composition

Gasification slag samples and residual carbons were subjected to wet sieving with 0.5 mm, 0.25 mm, 0.125 mm and 0.074 mm sets of sieves, respectively. The particle size composition of gasification slag and residual carbon products is shown in Table 2.

3.2.3. XRD analysis

The spectra of gasification slag and residual carbon are shown in Fig. 2. Two "steamed bread peaks" can be observed between 20° and 45° of 2θ, corresponding to the (002) crystal plane and the (101) crystal plane in the graphite XRD pattern, respectively. The (002) crystal plane of graphite is symmetrical, but the (002) crystal plane in the Fig. does not showed symmetry (Xiang et al., 2016). The wide and slow peak here was the result of the superposition of (002) crystal plane and γ band, in which (002) crystal plane was related to the degree of parallel orientation of aromatic structural units, and γ band is related

Table 2. Particle size composition of Gasification slag and residual carbon

Granularity/mm	Gasification slag		Residual carbon	
	Yield /%	Ash /%	Yield %	Ash /%
>0.5	1.26	95.02	--	--
0.25-0.5	3.05	48.66	3.61	14.54
0.125-0.25	6.22	46.48	43.69	13.65
0.074-0.125	15.24	69.63	52.70	17.83
<0.074	74.23	83.14	--	--
total	100.00	77.90	100.00	15.89
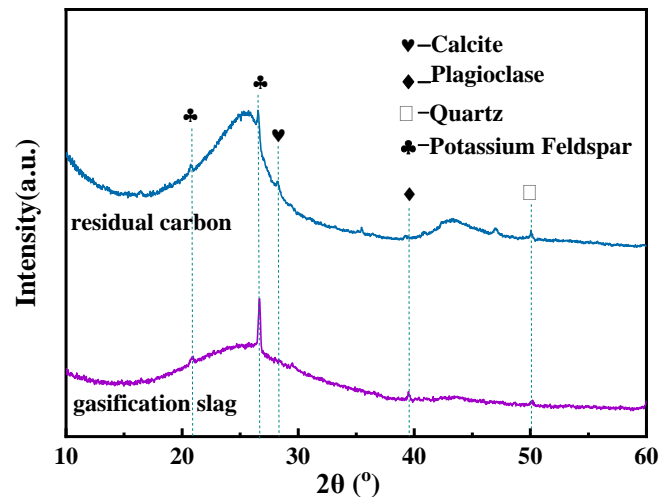
Fig. 2. Gasification slag and residual carbon mineral phase

to fatty carbon structure. It showed that the gasification slag and residual carbon contain a high proportion of amorphous phases such as aluminosilicate and amorphous carbon. Crystalline minerals are mainly quartz, calcite, plagioclase, potassium feldspar, etc. A small amount of calcite came from CaO (Shuai et al., 2015). The quartz characteristic peaks of residual carbon and gasification slag were obvious, and the characteristic peak of gasification slag calcite was more obvious than that of gasification slag, indicating that the proportion of calcite entering the residual carbon was larger after separation.

3.2.4. FT-IR Spectrum Analysis

The absorption spectra of gasification slag and residual carbon are shown in Fig. 3. It can be seen from the Fig. that there were obvious absorption peaks at 3700~3200 cm^{-1},1640~1540 cm^{-1}, 1250~1000 cm^{-1}, and the corresponding groups were -OH, -COOH and C=O, indicating that the surface of the residual carbon in the gasification slag contains a large number of oxygen-containing groups. More oxygen-containing functional groups result in enhanced hydrophilicity, which make it complicated to adhere to the bubbles, and the flotation effect becomes poor. At the same time, oxygen-containing groups will form intermolecular hydrogen bonds with water molecules, providing hydrophilic adsorption sited for water molecules and increasing the internal water content. There were two weak absorption peaks at 1650~1500 cm^{-1}, which were stretching vibrations of benzene ring skeleton, indicating that there were aromatic rings in the gasification slag, which was aromatic. Follow-up Raman spectroscopy can analyze the growth degree of aromatic rings. The gasification slag had weak absorption peaks at 475 cm^{-1} places, indicating the existence of inorganic minerals in the gasification slag, while the vibration intensity of the absorption peak in the residual carbon was weak, indicating that the gasification slag had achieved the removal of high-ash inorganic minerals through gravity separation.

It can be seen from the Fig. that there were obvious absorption peaks at 3700~3200 cm^{-1},1640~1540 cm^{-1}, 1250~1000 cm^{-1}, and the corresponding groups were -OH, -COOH and C=O, indicating that the

7

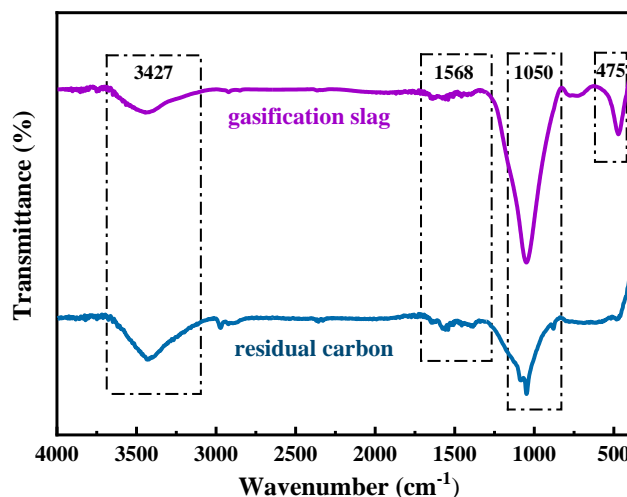Physicochem. Probl. Miner. Process., 58(6), 2022, 154928

Fig. 3. FT-IR spectrum of gasification slag and residual carbon

surface of the residual carbon in the gasification slag contains a large number of oxygen-containing groups. More oxygen-containing functional groups result in enhanced hydrophilicity, which made it complicated to adhere to the bubbles, and the flotation effect becomes poor. At the same time, oxygen-containing groups will form intermolecular hydrogen bonds with water molecules, providing hydrophilic adsorption sited for water molecules and increasing the internal water content. There were two weak absorption peaks at 1650~1500 cm^{-1}, which were stretching vibrations of benzene ring skeleton, indicating that there were aromatic rings in the gasification slag, which was aromatic. Follow-up Raman spectroscopy can analyze the growth degree of aromatic rings. The gasification slag had weak absorption peaks at 475 cm^{-1} places, indicating the existence of inorganic minerals in the gasification slag, while the vibration intensity of the absorption peak in the residual carbon was weak, indicating that the gasification slag had achieved the removal of high-ash inorganic minerals through gravity separation.

Table 3. Characteristic absorption peaks of FT-IR spectra of gasification slag and residual carbon (Miura et al., 2001; Jiang et al., 2019)

Serial number	Location /cm^{-1}	Functional group
1	3700~3200	-OH stretching vibration
2	3000~2843	Hydrocarbon C-H stretching vibration
3	1650~1500	Skeleton vibration of benzene
4	1250~1000	Alcohol C-O stretching vibration absorption peak
5	600~400	Clay mineral or carbonate mineral

3.2.5. Pore structure (low pressure gas adsorption) and SEM-EDS analysis

The adsorption-desorption curves and pore size distribution of the gasification slag and residual carbon were shown in Fig. 4, and the pore structure parameters were shown in Table 4. The microstructures of the gasification slag and residual carbon were shown in Fig. 5, and the SEM-EDS results were shown in Fig. 6.

It can be seen from the adsorption-desorption curves and pore size distribution diagrams of residual carbon and gasification slag that the adsorption and desorption curve conforms to type IV adsorption isotherm. The adsorption and desorption isotherms do not overlap, showing an obvious hysteresis loop. The hysteresis loop of the residual carbon is more obvious, and the pores with open permeability can produce hysterisis loop. It can be seen from the Fig. that the nitrogen adsorption capacity of the residual carbon was greater than that of the gasification slag indicating that the pore structure of the residual

(a) adsorption-desorption curves
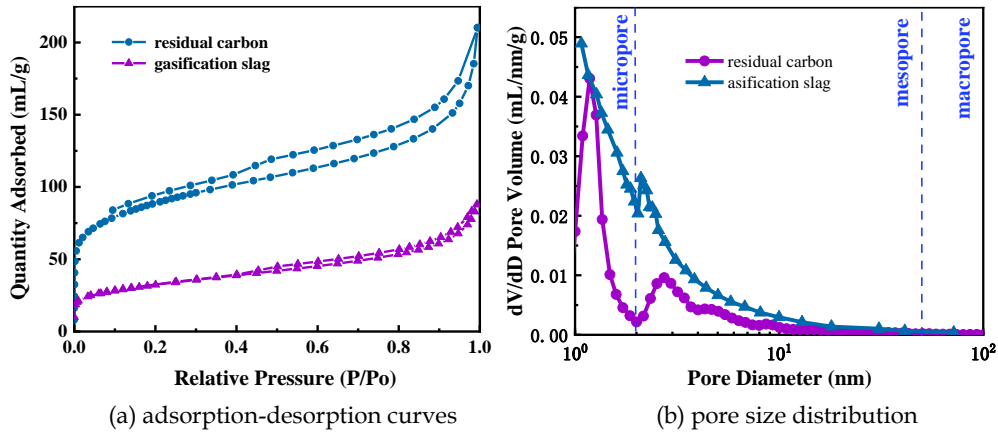
(b) pore size distribution

Fig. 4. Adsorption-desorption curves and pore size distribution of gasification slag and residual carbon

Table 4. Gasification slag and residual carbon pore structure parameters

Sample	BET specific surface area (m²/g)	Total pore volume (cm³/g)	Micropore pore volume (cm³/g)	Average pore size (nm)
Gasification slag	116	0.14	0.01	4.77
Residual carbon	296	0.31	0.09	5.57

carbon is more developed. The pore size of gasification slag and residual carbon was dominated by micropores, with a small amount of mesoporous structure. Table 4 showed the pore structure parameters of the two. The gasification slag had a certain pore structure due to the disappearance of the volatile matter in the pyrolysis stage and the reaction of the gasification agent through the char pores in the gasification stage. The residual carbon was obtained after the gasification slag was separated by water medium gravity. During the separation process, a large number of inorganic substances in the voids and voids were removed, and the proportion of amorphous carbon increased, resulting in an increase in porosity and the BET specific surface area from 116 m²/g to 296 m²/g. Fig. 5 SEM micrographs of gasification slag and residual carbon also confirm this point. Carbon is mainly irregular block, sheet and floc, with developed porosity. Spherical particles were inorganic minerals, which were fine molten particles formed by ash fusion polymerization in the process of coal gasification. More spherical particles of fine minerals were adhered and wrapped in the pores of gasification slag (Zhao et al., 2010). After separation, the spherical fine particles in the residual carbon products were obviously removed. The surface pore structure of residual carbon was relatively developed, with large porosity, large total pore area and strong adsorption capacity. For the flotation process of gasification slag, the developed pore structure will inevitably enhance the adsorption of water and reagent and increase the dosage of reagent.
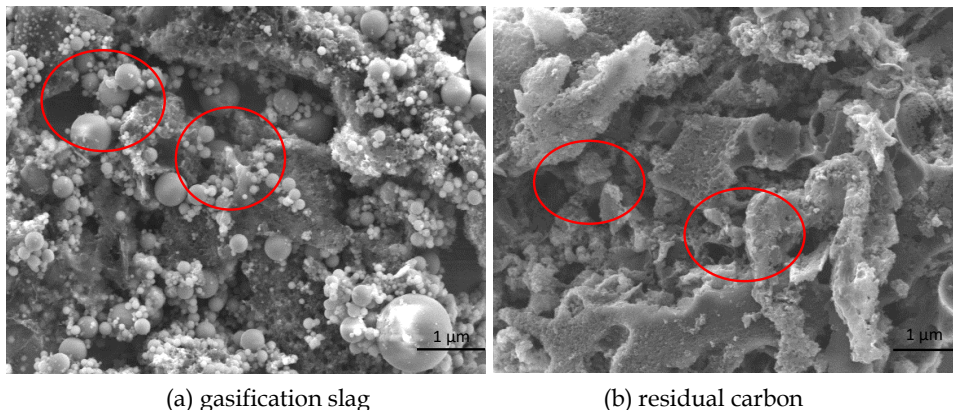
(a) gasification slag

(b) residual carbon

Fig. 5. SEM of gasification slag and residual carbon

(a) gasification slag   (b) residual carbon
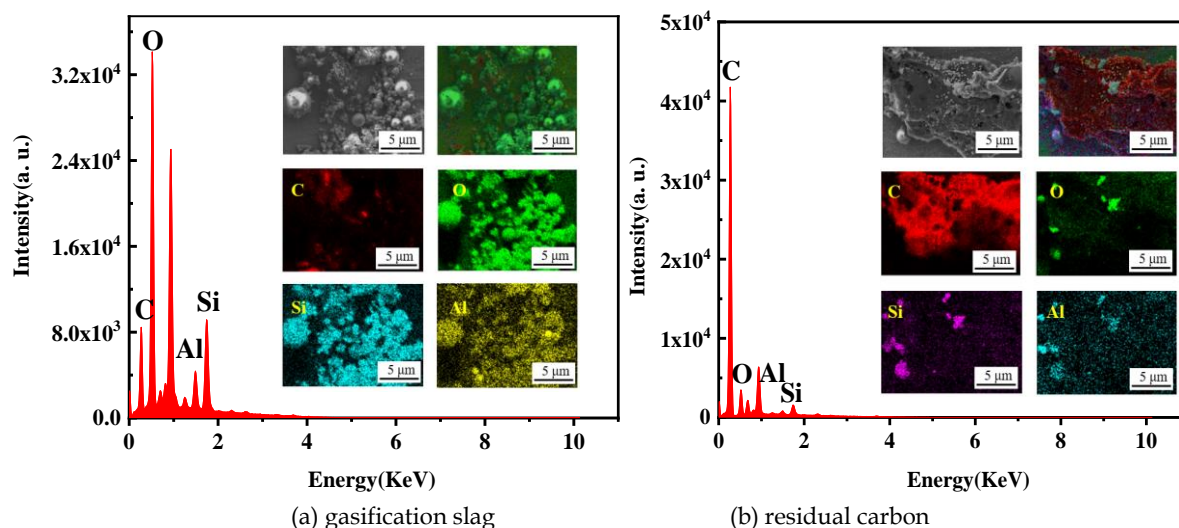
Fig. 6. SEM photos and EDS spectra of gasification slag and residual carbon

Fig. 6 shows the SEM-EDS results of the gasification slag and residual carbon. It can be seen from Fig. 6 that the spherical particles in the gasification slag were densely distributed, dominated by silicon-alumina oxides. After gravity separation, the larger particle spheres in the residual carbon were significantly reduced, and the C content was greatly increased, which has the potential to manufacture high value-added materials.

3.2.6. Raman analysis

There were two distinct peaks in Raman spectrum analysis, namely D peak and G peak, which were called "defect peak" and "graphite peak", respectively. For Raman spectroscopy of complex carbonaceous materials, many analytical methods were established. This section uses GRAMS software to fit 10 peaks for fitting analysis. The 10 peak positions and their representative structures were listed in Table 5.

The Raman spectral curve was fitted by peaks, as shown in Fig. 7, and the fitting parameters of each peak were shown in Table 6. The Raman intensity was affected by the oxygen-containing functional group, and the loss of the oxygen-containing functional group will greatly reduce the resonance effect between the oxygen-containing functional group and the aromatic ring structure, thereby reducing the Raman peak intensity. The full width at half maximum of the G peak ($FWHM\text{-}G$) indicates the degree of aromatization of the sample. The smaller the full width at half maximum of the G peak, the higher the degree of aromaticity and the higher the degree of graphitization. $(A_{GR}+A_{VL}+A_{VR})/A_D$ discriminates

Table 5. band assignment of Raman spectrum (1800~800 cm^{-1})

Peak name	Peak location /cm^{-1}	Reflected structural information	Key type
G_L	1700	C=O	sp^2
G	1590	C=C，E_{2g}^2vibrations of the aromatic ring plane	sp^2
G_R	1540	3-5 ring aromatic rings	sp^2
V_L	1465	Amorphous carbon structure	sp^2、sp^3
V_R	1415	Methyl, methylene functional groups or semicircular aromatic ring vibrations	sp^2、sp^3
D	1350	Aromatic hydrocarbons	sp^2
S_L	1230	Aryl alkyl ether	sp^2、sp^3
S	1185	C-C between aryl and alkyl and C-H on aromatic ring	sp^2、sp^3
S_R	1060	C-H on the aromatic ring	sp^2
R	960~800	C-C of alkanes and cyclic alkanes	sp^2、sp^3

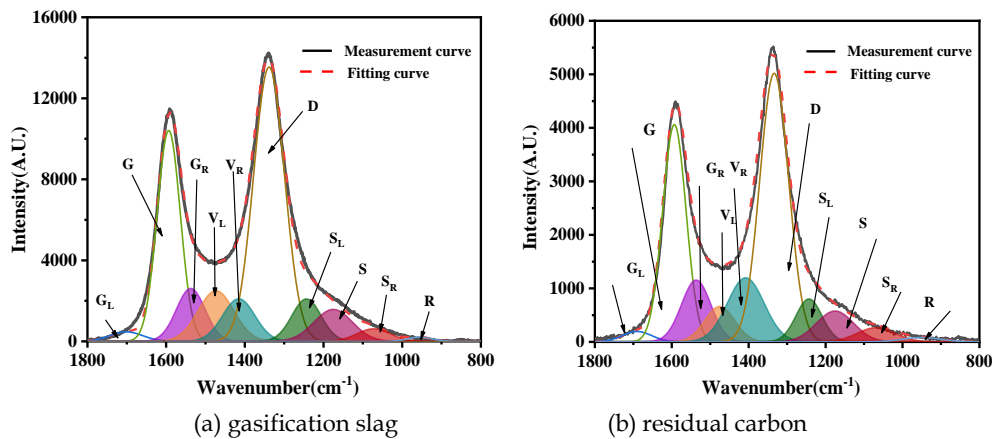(a) gasification slag   (b) residual carbon

Fig. 7. Raman spectral curve of gasification slag and residual carbon

the ratio of different types of aromatic rings, representing the ratio of the small ring structure of 3-5 aromatic rings and the macrocyclic structure of ≥6 aromatic rings (Li et al.,2021). Among them, A_{GR} - peak area corresponding to 3-5 aromatic rings in the Raman spectrum; A_{VL} - peak area corresponding to amorphous carbon structure in the Raman spectrum; A_{VR} - peak area corresponding to methyl, methylene functional groups or semicircular aromatic ring vibrations in the Raman spectrum; A_D - peak area corresponding to graphite defect structure reflected by D peak in highly ordered carbon materials or C-C structure between aromatic rings with no less than 6 rings in the Raman spectrum. Literature shows (Han et al.,2016), The ignition temperature of the sample increases with the increase of the aromaticity of the sample, and the ratio of the content of small and large ring structures and the pore structure together affect the burnout temperature. Comparing the Raman spectral parameters of the residual carbon and the gasification slag, see Table 6, it can be observed that the *FWHM-G* and $(A_{GR}+A_{VL}+A_{VR})/A_D$ of the two samples was that gasification slag was smaller than residual carbon, which proves that the aromaticity of gasification slag was higher, the content of large aromatic ring structure was higher, and the larger aromatic ring forms carbon crystals with more ordered and directional structure. Combined with the SEM-EDS analysis results, it can be seen that the proportion of amorphous carbon in the residual carbon was higher than that in the gasification slag, which also confirms that the gasification slag was more ordered than the residual carbon.

3.2.7. Thermogravimetric analysis and combustion kinetics

As shown in Fig. 8(a), where T_i was the ignition temperature, on the DTG curve, the point a passing the

Table 6. Raman Spectral Parameters of Gasification slag and Residual carbon

Sample	*FWHM-G*/cm⁻¹	A_D/A_G	$(A_{GR}+A_{VL}+A_{VR})/A_D$
Gasification slag	71.51	1.86	0.38
Residual carbon	77.24	1.60	0.48

Note: *FWHM-G* is the full width at half maximum of G peak; A_D/A_G is the ratio of the areas of D peak and G peak; $(A_{GR}+A_{VL}+A_{VR})/A_D$ is the ratio of the sum of the areas of G_R peak; V_L peak and V_R peak to the area of D peak.

peak value is taken as the vertical line to intersect the TG curve at point B. the tangent of TG curve passing through point B intersects the horizontal straight line after dehydration drying at point C. The temperature corresponding to point C is the ignition temperature. T_h was the burnout temperature, after this point, the TG curve no longer has mass change (Lv et al.,2021). It can be seen from Fig. 8(b) that the combustion mainly goes through three stages. The first stage was the drying stage of dehydration, which was mainly the removal of adsorbed water. The temperature range is 35~300 ℃.The second stage was the combustion stage of volatilization analysis, and the temperature range is about 400~650 ℃.After the first peak of the DTG curve appears, the weight loss rate gradually decreases, and the weight loss tends to be gentle on the TG curve. When the combustion progresses to a certain extent, the fixed carbon

begins to burn, that was, it enters the third stage of fixed carbon combustion. The temperature range is about 400 ~ 650 ℃, until the final fixed carbon burns out. The larger the peak value of DTG curve, the longer the duration, indicating that the product burns more violently and is more resistant to
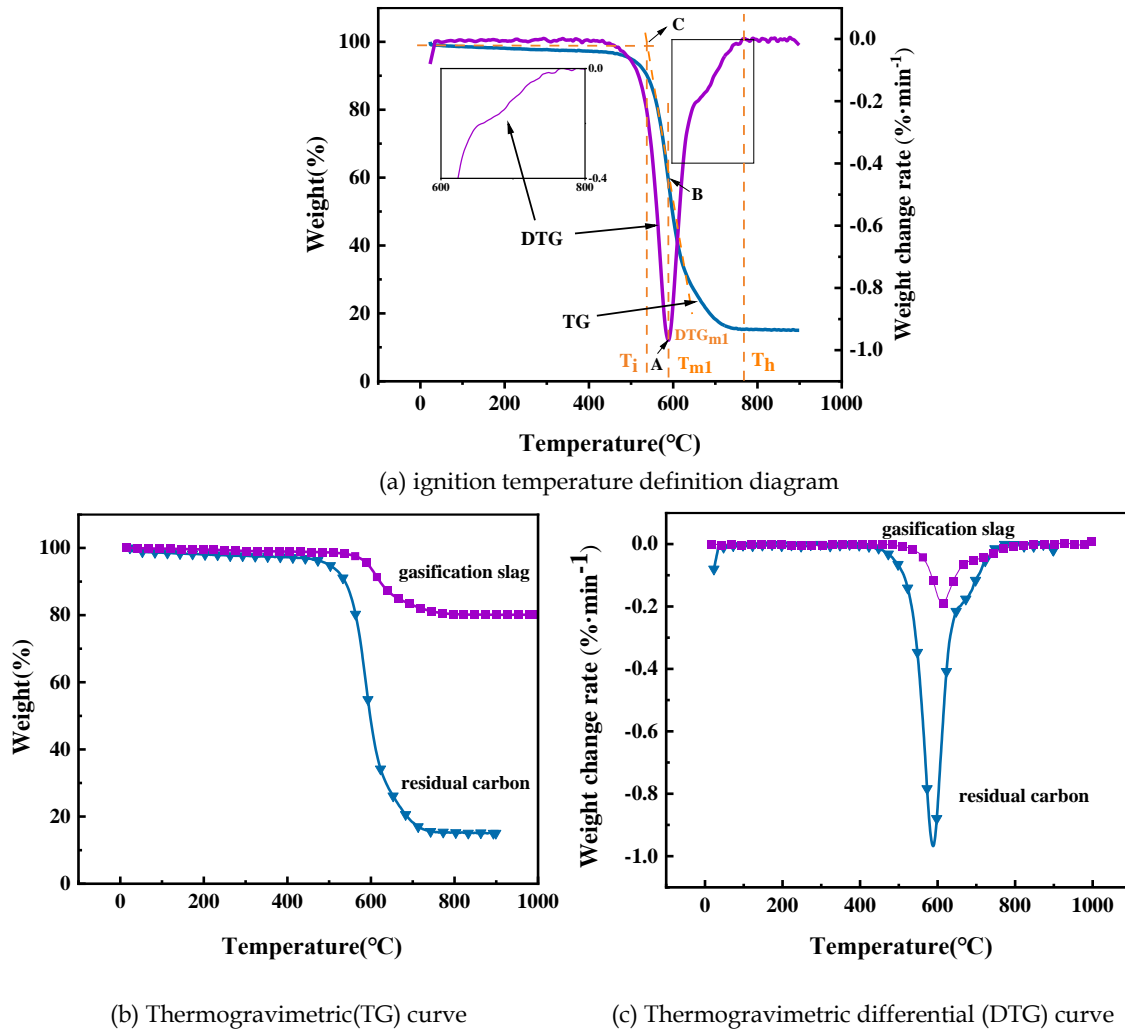

(a) ignition temperature definition diagram

(b) Thermogravimetric(TG) curve

(c) Thermogravimetric differential (DTG) curve

Fig. 8. Ignition temperature definition diagram and thermogravimetric analysis curve of residual carbon and gasification slag

combustion. The peak value of residual carbon is larger than that of gasification slag, which indicates that residual carbon is more conducive to stable combustion than gasification slag. Among them, the weight loss of residual carbon is significantly greater than that of gasification slag, and the burnt out material is only 16%, which indicates that some minerals of gasification slag are removed through water-based gravity separation, which is more conducive to fully contact with oxygen and promote oxygen to move to the carbon surface.

By observing Fig. 8 and calculating the residual carbon combustion characteristic values in Table 7. Among them, S is the comprehensive combustion characteristic index, and the calculation method is shown in formula (2).

$$S = \frac{(\mathrm{d}m/\mathrm{d}t)_{\mathrm{mean}}(\mathrm{d}m/\mathrm{d}t)_{\mathrm{max}}}{T_i^2 T_h} \tag{2}$$

In the process of combustion reaction, the activation energy E represents the difficulty of the reaction, and the frequency factor A represents the degree of the chemical reaction per unit time. The two together affect the reaction rate. In this paper, the integral method was used to process the kinetic experimental data during the combustion of residual carbon to obtain the activation energy E and frequency factor A.

The residual carbon conversion rate a, as shown in formula (3).

Table 7. Combustion characteristics of gasification slags and residual carbons

Sample	T_i/°C	T_h/°C	DTG_{m1}/ % ·min⁻¹	T_{m1}/°C	DTG_{m2}/ % ·min⁻¹	T_{m2}/°C	$(dm/dt)_{mean}$/ % ·min⁻¹	S/ % ²·min⁻²·°C⁻³
Gasification slag	569	820	0.188	612	0.074	745	0.135	$9.56 \cdot 10^{-11}$
Residual carbon	538	768	0.967	588	0.215	652	0.325	$1.41 \cdot 10^{-9}$

Note: T_i is the ignition temperature; T_h is the Burnout temperature; DTG_{m1} is the The maximum precipitation rate of volatile analysis; T_{m1} is the peak temperature in the combustion stage of volatilization analysis; DTG_{m2} is the fixed carbon maximum burning rate; T_{m2} is the peak temperature in the combustion stage of fixed carbon; $(dm/dt)_{mean}$ is the average burn rate; S is the comprehensive combustion characteristic index.

$$\alpha = \frac{m_0 - m_t}{m_0 - m_f} \tag{3}$$

In the formula, m_0 is the initial mass, mg; m_t is the mass of sample after time t, mg; m_f is the weight of the ash in the sample, mg.

For n-order reactions, there is the burning rate equation (4).

$$\frac{d\alpha}{dt} = k(1-a)^n = \frac{A}{\gamma} e^{-E/RT}(1-a)^n \tag{4}$$

In the formula, k is the reaction rate constant, obeying Arrhenius' law: $k=Ae^{-E/RT}$, A is the frequency factor，min⁻¹; E is the activation energy of the reaction, kJ/mol；R is the gas constant , 8.314 J/(mol⁻¹·K⁻¹); T is the absolute temperature; γ is the heating rate of thermal re-combustion, which is 5 °C/min in this experiment.

For general combustion, it can be treated as a first-order reaction. In this paper, it is assumed that the volatilization analysis of the residual carbon shows that the combustion process and the fixed carbon combustion process were both first-order reactions, that is, $n=1$, and the integration method is used to integrate both ends of Equation (4) to obtain:

$$\ln\left[-\frac{\ln(1-a)}{T^2}\right] = \ln\left[\frac{AR}{\gamma E}\left(1-\frac{2RT}{E}\right)\right] - \frac{R}{ET} \tag{5}$$

In the formula, $1 - \frac{2RT}{E}$ is approximately equal to 1, Draw a straight line to $1/T$ through $\ln\left[-\frac{\ln(1-\alpha)}{T^2}\right]$, Rewriting formula (5) as: $y=kx+b$，the frequency factor A can be obtained from the slope k of the straight line, and the activation energy E can be obtained from the intercept b of the straight line. The reaction kinetic parameters of the volatile analysis combustion process and the fixed carbon combustion process obtained according to the above method were shown in Table 8.

Table 8. Combustion kinetic parameters of gasification slag and residual carbon

Sample	T/°C	Correlation equation	E/kJ·mol⁻¹	$\ln A$	R
Gasification slag	569~660	34.341-21508x	178.81	27.93	0.964
	661~820	18.735-13681x	113.74	18.92	0.956
Residual carbon	538~625	35.987-21366x	177.63	36.17	0.975
	626~768	19.360-13233x	110.02	19.54	0.961

It can be seen from the data in Table 8 that the combustion process curve consists of two straight lines with different slopes, and the linear correlation was good, and the correlation coefficients were all above 0.95, which satisfies the first-order reaction equation, indicating that the assumed first-order reaction mechanism was reasonable. The activation energy and frequency factor in the fixed carbon combustion stage were smaller than those in the volatile analysis combustion stage, which proves that the fixed carbon combustion reaction was easier than the volatile analysis combustion.

It can be seen from Fig. 8 combined with Table 7 and Table 8 that after separation and upgrading, the ignition temperature T_i of the residual carbon decreased from 569 °C to 538 °C, the burnout

temperature T_h decreased from 820 °C to 708 °C. The average combustion rate increased from 0.135% min^{-1} to 0.325% min^{-1}, the comprehensive combustion characteristic index increased, and the peak temperature T_{max} and the activation energy E of the two stages were lower than those of the gasification slag, while the frequency factor A was higher than that of the gasification slag. From this, it can be seen that, compared with the gasification slag, the residual carbon has lower ignition difficulty, higher burnout ability, and excellent combustion performance. The aroma of gasification slag was greater than that of residual carbon, which also confirms that the ignition temperature of gasification slag was high. Compared with gasification slag, the more developed pore structure of residual carbon was beneficial to the mass and heat transfer in the combustion process. The ash content of the residual carbon was lower, the combustible substances were relatively increased, the calorific value was increased, and the ignition and combustion of the residual carbon were affected, so that the combustion efficiency was increased. In addition, combined with the results of Raman spectroscopic analysis, the residual carbon has a higher content of small and medium aromatic ring structures, low structural stability, less chemical activation energy, the content of amorphous carbon structure was high, and the combustion was easier, which also confirms that the combustion characteristic index of residual carbon was higher than that of gasification slag.

4. Prospect and reflection on the utilization direction of residual carbon

According to the analysis and characterization of the physicochemical properties of the residual carbon, residual carbon has a certain pore structure and large specific surface area, which can be used as an adsorbent to treat industrial wastewater, and as a raw material to prepare high-efficiency and low-cost deodorants, activated carbon, activated coke, etc. The process cost was low, and it has certain social and economic benefits. The developed pore structure has the potential to store and release humic acid, and was expected to become a humic acid slow-release agent to improve the physical and chemical properties of soil. It can not only realize the large-scale consumption of gasification slag, but also have a good effect on ecological restoration. The residual carbon has high burning vector, high burnout capacity, excellent combustion performance and high combustion characteristic index. According to the requirements of the minimum calorific value of the feed of the circulating fluidized bed boiler is 14.64 MJ kg^{-1}, the calorific value was greater than the minimum requirements of circulating fluidized bed boiler. It can also be directly used as mixed combustion raw material for mixed combustion of circulating fluidized bed to reduce carbon dioxide emission and realize the comprehensive utilization of residual carbon resources.

5. Conclusion

Through the research on the basic physical properties of the fine slag obtained from a chemical base in northern China, the following conclusions were drawn:

1. The carbon-ash separation of a chemical base in northern China gasification fine slag was carried out by water medium gravity separation to obtain residual carbon products, ash-rich products with fine particle size that need further separation, and high-ash products with low LOI. Under the optimal structure of this study, the yield of residual carbon was 11.64%, the ash content was 16.84%, and the distribution rate of residual carbon was 40%. The separation effect was good, and the high-efficiency carbon-ash separation of coal gasification slag was realized.

2. XRD and SEM-EDS spectra show that the residual carbon has a higher proportion of amorphous carbon and higher carbon content compared with the gasification slag. It can be seen from the BET pore structure theoretical model that the residual carbon was mainly mesoporous. Higher carbon content and more developed pore structure provide the possibility of high value-added utilization of residual carbons. It has the potential to manufacture adsorbent, activated carbon, activated coke and other materials, with low process energy consumption and certain social and economic benefits.

3. The comparative analysis of carbon residue and gasification slag by Raman spectroscopy combined with thermogravimetric method showed that the *FWHM-G* of carbon residue was larger than that of gasification slag, Residual carbon had a lower degree of aromaticity, a lower degree of graphitization, a more stable structure and a lower ignition temperature. The $(A_{GR}+A_{VL}+A_{VR})/A_D$ of the carbon residue was larger than that of the gasification slag, and the content of small and medium

aromatic ring structure in residual carbon was higher. The content of medium and small ring structure and mesoporous structure together reduced the ignition temperature of residual carbon. The excellent combustion performance of residual carbon can be used for mixing raw materials in a circulating fluidized bed.

4. Combined with the physical characteristics of gasification slag carbon, we should continue to explore new fields of high-value utilization, which can realize the comprehensive utilization of solid waste resources, meet the needs of social development, ease the pressure on the environment, and obtain good economic and environmental benefits.

Acknowledgments

References

AYENI, J. O.; MA, S. H.; WANG, X. H.; HOU, X. 2022, *A Facile Synthesis Process and Electromagnetic Absorption Performance of High Alumina Fly Ash and Gasification Slag- Based Ceramic Composite*s. J. Available at SSRN 4102978.

BLISSETT, R.S.; ROWSON, N.A. 2012, *A review of the multi-component utilisation of coal fly ash*. J. Fuel. 9, 1–23.

BASTRZYK, A., POLOWCZYK, I., SADOWSKI, Z., SIKORA, A., 2011. *Relationship between properties of oil/water emulsion and agglomeration of carbonate minerals.* Sep. Purif. Technol. 77, 325-330.

CHAO, Y. J.; WANG, H. J. 2015, *Feasibility Study of Circulating Fluidized Bed Boiler Blending Burning Gasification Slag and Coal Slime.* J. Chemical Fertilizer Industry. 48-50.

DONG, L. P.; *A method for efficiently classifying coal gasification waste residue to prepare high-purity ash and high-purity carbon*:CN201810013201.3. P. 2018-06-15.

DONG, L. P.; FAN, P. P.; FAN, M. Q. *A kind of gasification slag hydrocyclone gravity separation carbon ash separation device and method*:CN111659527A. P.2020-09-15.

DRZYMALA, J., 2007. *Mineral processing. Foundations of theory and practice of minerallurgy.* Ofic. Wyd. PWr, Wroclaw, Poland.

EMRE ALTUN, N.; XIAO C.F.; HWANG, J.Y. 2009, *Separation of unburned carbon from fly ash using a concurrent flotation column*. J. Fuel Processing Technology. 90, 1464-1470.

FLORENCE, T.; ANDREI, VEKSHA.; VICTOR W.K.; C.; W.D. CHANAKA, U.; DARA, K.; BINTE, M.; APOSTOLOS, G.; TEIK-THYE, L.; GRZEGORZ, L. 2019, *Nickel-based catalysts for steam reforming of naphthalene utilizing gasification slag from municipal solid waste as a support*. J. Fuel. 254, 115561.

GUO, F. H.; ZHAO, X.; GUO, Y.; ZHANG, Y. X.; WU, J. J. 2020, *Fractal analysis and pore structure of gasification fine slag and its flotation residual carbon*. Colloids and Surfaces A: Physicochemical and Engineering Aspects. J. 585, 124148.

HAN, Y. N.; LIAO, J. J.; BAI, Z. Q.; BAI, J.; LI, X.; LI, W. 2016, *Correlation between the Combustion Behavior of Brown Coal Char and its Aromaticity and Pore Structure*. Energy & Fuels, 30, 3419-3427.

HE, X. W.; CUI, W.; WANG, C. R.; SHI, Y. T.; ZHANG, J. 2014, *Leaching characteristics and chemical speciation analysis of heavy metals in gasification furnace slag*. J. Chemical environmental protection. 34, 499-502.

HU, Z. W.; LIU, T.; MAN, J.; LV, Q. L. 2016, *Sources of main environmental pollutants in coal chemical industry and pollution control countermeasures*. J. Shandong chemical industry. 45, 155-156,158.

HU, J. Y.; HUANG, Y.; WANG, W. Q.; FENG, Q. M.; XU, Z. H. 2018, *Application of coal gasification slag flotation fine carbon in dyeing wastewater*. J. Environmental engineering. 36 (3): 59-63

JIANG, J, Y.; YANG, W, H.; CHENG, Y, P.; LIU, Z, D.; ZHANG, Q.; ZHAO, K. 2019, *Molecular structure characterization of middle-high rank coal via XRD, Raman and FTIR spectroscopy: Implications for coalification*. J. Fuel. 239: 559-572.

LIU, D. X.; HU, J. Y.; FENG, Q. M.; HUANG, Y.; XU, Z. H.; 2018, *Study on Flotation of Coal Gasification Slag and Preparation of Activated Carbon from Carbon Concentrate*. J. Coal Conversion. 41, 73-80.

LIU, X. D.; JIN, Z. W.; JING, Y. H.; FAN, P. P.; QI, Z. L.; BAO, W. R.; WANG, J. C.; YAN, X. H.; LV, P.; DONG, L. P. 2021, *Review of the characteristics and graded utilisation of coal gasification slag*. J. chinese journal of chemical engineering. 35, 92-106.

LI, H. Z.; DONG, L. P.; BAO, W. R.; WANG, J. C.; FAN, P. P.; FAN, M. Q. 2021, *Cyclone carbon ash separation of coal gasification slag water medium based on apparent density*. J. Progress in chemical industry. 1344-1353.

LI, H. T.; CAO, D. Y.; ZHANG, W. G.; WANG, L. 2021, *XRD and Raman spectroscopic characterization of graphitization trajectory of high coal grade coal*. J. Spectroscopy and spectral analysis, 41 (8): 2491-2498.

LV, D. P.; BAI, Y. H.; WANG, J. F.; SONG, X. D.; SU, Z. G.; YU, G. S.; ZHU, H.; TANG, G. J. 2021, *Study on structural characteristics and combustion characteristics of residual carbon in entrained flow gasification fine slag*. J. Journal of Fuel Chemistry and Technology, 49, 129-136.

MIURA, K.; MAE, K.; LI, W.; KUSAKAWA, T.; MOROZUMI, F. 2001, *A Kumano Estimation of hydrogen bond distribution in coal through the analysis of OH stretching bands in diffuse reflectance infrared spectrum measured by in-situ technique*. J. Energy & Fuels. 15(3): 599-610.

POMYKALA, R. 2014, *The Mechanical properties of coal gasification slag as a component of concrete and binding mixtures.* J. Polish Journal of environmental studies. 23, 1403-1406.

REN, Z. Y.; JING, Y. H.; FAN, P. P.; GAO, Y. C.; WANG, J. C.; DONG, L. P.; BAO, W. R.; FAN, M. Q.; CHANG, L. P. 2021, *Experimental study on the water medium gravity separation of gasification slag and the preparation of desulfurization and denitrification activated coke using separated carbon*. J. Journal of China Coal Society, 46, 1164-1172.

SHI, Z. C.; DAI, G. F,; WANG, X. B.; DONG, Y. S.; LI, P.; YU, W.; TAN, H. Z. 2020, *Review on the comprehensive resources utilization technology of coal gasification fine slag*. J. Huadian Technology. 42, 63-73.

SHUAI, H.; YIN, H. F.; YUAN, H. D.; CHEN, J. X.; 2015, *High temperature phase composition evolution and viscosity temperature characteristics of coal gasification slag*. J. Coal conversion, 38, 44-48.

WANG, F. C. 2021.*Coal gasification technology in China: review and prospect*. J. Clean coal technology.27, 1-33

WANG, X. B.; FU, J. G.; ZHAO, D.; HUANG, Y. T. 2021, *Study on flotation quality improvement of fine slag carrier*. Coal engineering. J. 53, 155-159.

WANG, J. KONG, L. X.; BAI, J.; LI, H. Z.; GUO, Z. X.; BAI, Z. Q.; Li W. 2021, *Research Progress on the influence of residual carbon in coal gasification ash on ash fluidity*. J. Clean coal technology, 27, 181-192.

WU, S. P.; ZHAO, K.; DONG, Y. S.; WANG, X. B.; BAI, Y. H.; LIU, L. J.; YU, W. 2020, *Research progress on flotation decarburization of gasification fine slag*. J. Huadian Technology. 42, 81-86.

VASSILEV, S.V.; MENENDEZ, R.; BORREGO, A.G. 2004, *Phase-mineral and chemical composition of coal fly ashes as a basis for their multicomponent utilization. 3. Characterization of magnetic and char concentrates*. J. Fuel and Energy Abstracts.83, 1563-1583.

XIANG, J. H.; ZENG, F. G.; LIANG, H. Z.; LI, M. F.; SONG, X. X.; ZHAO, Y. Y. 2016, *Carbon structure characteristics and evolution mechanism of coals with different metamorphic degrees*. J. Journal of China Coal Society, 41, 1498-1506.

XU, S.; ZHOU, Z.; GAO, X.; YU, G. S.; GONG, X. 2009, *The gasification reactivity of unburned carbon present in gasification slag from entrained-flow gasifier*. J. Fuel Processing Technology. 90, 1062-1070.

XUE, Z. H.; DONG, L. P.; LIU, A.; FAN, M. Q.; YANG, C. Y.; WANG, J. C.; BAO, W. R.; FAN, P. P. 2022, *Feasibility and mechanism analysis of hydrophobic hydrophilic two-liquid separation of gasification fine slag*. J. Journal of China Coal Society, 1-12.

XUE, Z. H.; DONG, L. P.; FAN, M. Q.; YANG, H. L.; LIU, A.; LI, Z. H.; BAO, W. R.; WANG, J. C.; FAN, P. P. 2021. *Enhanced flotation mechanism of coal gasification fine slag with composite collectors*, Colloids and Surfaces A: Physicochemical and Engineering Aspects, 2022.128593

YANG, S.; SHI, L. J.; 2013, *Component analysis and comprehensive utilization of coal gasification fine slag*. J.Coal chemical industry. 4, 34-36,43

YU, W.; WANG, X. B.; BAI, Y. H.; LIU, L. J.; SHI, Z. C.; ZHAO, Y. X.; TAN, H. Z. 2021, *Experimental study on flotation decarbonization of coal gasification fine slag*. J. Clean coal technology. 27, 81-87

ZHAO, X. L.; ZENG, C.; MAO, Y. Y.; LI, W. H.; PENG, Y.; WANG, T.; EITENEER, B. 2010, *The Surface Characteristics and Reactivity of Residual Carbon in Coal Gasification Slag*. J. Energy & Fuels, 24, 91-94.

ZHU, D. D.; MIAO, S. D.; XUE, B.; JIANG, Y. S.; WEI, C. D. 2019, *Effect of Coal Gasification Fine Slag on the Physicochemical Properties of Soil*. J. Water, Air, & Soil Pollution. 230